RSC Advances

ROYAL SOCIETY OF CHEMISTRY

www.rsc.org/advances

Journal Name

ARTICLE

Photoelectrochemical Cell for Unassisted Overall Solar Water Splitting Using $BiVO_4$ Photoanode and Si Nanoarray Photocathode

Received 00th January 20xx,
Accepted 00th January 20xx

DOI: 10.1039/x0xx00000x

www.rsc.org/

Pan Xu,[a] Jianyong Feng,[a] Tao Fang,[a] Xin Zhao,[a] Zhaosheng Li,[a,*] Zhigang Zou[a,b]

Overall solar water splitting without external bias was demonstrated in this study using a photoelectrochemical tandem device of $BiVO_4$ photoanode and Si nanoarray photocathode. An unassisted photocurrent density of 0.6 mA cm^{-2} is possible under AM 1.5G illumination, by examining the current density-voltage curves of respective photoelectrodes and the operating point in three-electrode system. We then investigated the unassisted two-electrode operation of the tandem cell, and a solar-to-hydrogen efficiency of 0.57 % (corresponding photocurrent density of 0.46 mA cm^{-2}) was achieved under AM 1.5G illumination (100 mW cm^{-2}). The solar photocurrent density of this tandem cell decayed during the stability testing, possibly due to the dissolution of Co-Pi electrocatalyst rather than the instability of p-Si photocathode.

1. Introduction

Hydrogen is a promising candidate as a future clean energy carrier if it can be produced using the abundant sunlight. Photoelectrochemical (PEC) water splitting is considered a potential strategy for solar-to-hydrogen (STH) conversion, and has attracted intense attention. [1-7] An ideal STH conversion device should be low-cost, environmentally safe, and efficient enough for applications on medium and large scales. [8-11] Although only about 1.6–1.8 V of photopotential is pre-requisite to surmount the thermodynamic and kinetic barriers of water splitting, an individual photoelectrode with high STH conversion efficiency has not been realized because large external bias is required for overall water splitting. [12, 13] Therefore, novel approaches to achieve efficient PEC water splitting without external bias are strongly desired.

One feasible approach is the combination of photoelectrodes and photovoltaic (PV) cells, which is called as PEC-PV tandem cell. [14-23] This type of tandem cell can achieve relatively high efficiency but usually require complicated setups and solar cells with a high open-circuit voltage. Classic examples of such tandem cells include a crystalline p-$GaInP_2$ photocathode in contact with a GaAs solar cell.[22] In addition, the high cost of the solar cells and complex electrical connections in these systems limit their large-scale practical application. Thus, a trade-off between maximizing device performance and minimizing system complexity (i.e., device cost) must be made in any PEC system for STH conversion on a certain scale.

An alternative PEC-based approach for water splitting is to use a photocathode and a photoanode connected in series to form a p-n PEC tandem cell. [24-27] In this configuration, solar photons that are not absorbed by the top electrode are transmitted and absorbed by the bottom electrode. In this setup, two semiconductors with smaller band gaps than that of the semiconductor in a single photoelectrode may be adopted, because each only needs to provide part of the water splitting potential. The smaller band gaps increase absorption in the visible region of the solar spectrum, which possesses the majority of the photon flux from the sun. Such a tandem cell is theoretically possible only if the conduction band minimum of the photoanode lies at lower electrochemical potential than the valence band maximum of the photocathode. Therefore, the proper selection of both semiconductor electrodes should ensure that the energy necessary for water splitting is gathered entirely from the light source, eliminating the need to apply electrical energy from an external source. In this system, water splitting potential is generated directly at the semiconductor–liquid interfaces to oxidize and reduce water. This minimizes the number of junctions used, making the device simpler and potentially cheaper.

Si is currently the leading material in the PV industry because of a vast knowledge base and manufacturing infrastructure arising from its abundance and relatively low cost. [28-30] The promising photocathode performance of p-type Si (p-Si) nanoarrays with a preferred geometry may be used to produce inexpensive photoanode/photocathode tandem cells. [31-36] $BiVO_4$ is a suitable tandem partner for p-Si, because of its photoresponse up to 510 nm, high stability in neutral pH solution and relatively suitable onset of anodic photocurrent compared with other oxide photoanode materials like TiO_2,

[a] Collaborative Innovation Center of Advanced Microstructures, National Laboratory of Solid State Microstructures, and College of Engineering and Applied Sciences, Nanjing University, 22 Hankou Road, Nanjing, Jiangsu 210093, P.R. China
[b] Department of Physics, Nanjing University, 22 Hankou Road, Nanjing 210093, P.R. China

† Footnotes relating to the title and/or authors should appear here.
Electronic Supplementary Information (ESI) available: [details of any supplementary information available should be included here]. See DOI: 10.1039/x0xx00000x

Fe_2O_3 and WO_3.[37-42] Herein, we have examined the feasibility of a $BiVO_4$/Si nanoarray tandem cell for unassisted overall water splitting in aqueous potassium phosphate solution (pH=5.5). Analysis of the current–voltage (*J*-V) curves of the two photoelectrodes before and after the stability testing provides important insights into the routes to further improve this tandem cell.

2. Experimental

2.1 Fabrication of the Pt/Si nanoarray photocathode

The p-Si nanoarray photocathode was fabricated by metal-catalyzed electroless etching and then decorated with Pt electrocatalyst. [43-45] The p-Si wafer (Hefei Kejing Inc., 1–10 Ω•cm, (1 0 0) orientation, B-doped) was cleaned by ultrasonication in acetone for 10 min, ethanol for 10 min and deionized water for 5 min, and then chemically etched by immersion in a mixture of H_2SO_4 and H_2O_2 (1:3 v/v) for 30 min followed by immersion in 5% HF for 1 min to etch surface oxide. Then the clean p-Si wafer was put in a vessel containing an etching solution of 5 M HF and 0.02 M $AgNO_3$ for 30 min at 50 °C. After the reaction, the Ag dendrites formed on the surface of the p-Si nanoarray surface were removed by immersing the sample in a mixture of HNO_3 and H_2O_2 (1:1 v/v). An ohmic contact was fabricated by depositing a 500-nm Au film on the back of the p-Si substrate and annealing in N_2 at 400 °C for 2 min. For measurements in solution, the back of the p-Si sample was electrically connected to a Cu wire using Ag conductive adhesive. The contact area was electrically sealed using an epoxy resin, except for an area of 1 cm^2 that was defined as the projected area of the photocathode.

Before Pt decoration, the Si photocathodes were washed in concentrated HNO_3 for at least 1 h to remove all Ag from the surface of the nanoarray. Photoassisted electrodeposition of Pt onto the surface of the Si nanoarray photocathode was performed in a solution of 5 mM H_2PtCl_6 under AM 1.5 G simulated sunlight illumination at a constant potential (−0.03 V vs. Ag/AgCl) for 200 s.

2.2 Fabrication of the Co-Pi/Mo:$BiVO_4$ photoanode

Mo-doped $BiVO_4$ photoanodes were synthesized by a modified metal–organic decomposition method based on our previous work. [37] $Bi(NO_3)_3$•$5H_2O$ in glacial acetic acid (0.2 mol L^{-1}), vanadyl acetylacetonate in $CH_3COCH_2COCH_3$ (0.03 mol L^{-1}) and molybdenyl acetylacetonate in $CH_3COCH_2COCH_3$ (0.01 mol L^{-1}) were used as starting solutions. These solutions were mixed together well to give a stoichiometric ratio of Bi:V:Mo of 100:97:3. The mixed solution (~55 µL) was added dropwise onto a FTO (SnO_2: F) substrate (1 × 1.5 cm^2), dried and then calcined at 470 °C in a muffle furnace for 30 min to form Mo:$BiVO_4$ films. [37]

Co-Pi catalyst was deposited on the photoanode by photoassisted galvanostatic electrodeposition with a fixed current of 10 µA under AM 1.5 G illumination for 400 s in a three-electrode cell. [46] The cell contained electrolyte composed of 0.5 mM $Co(NO_3)_2$ (Guanghua Sci-Tech Co., China, >99%) and 0.1 M potassium phosphate (Nanjing Chemical Co., China, >99%) solution buffered to pH 7 with 1 M KOH (Nanjing Chemical Company, China, >85%).

2.3 Characterization of samples

The morphologies of the samples were examined with a scanning electron microscope (FESEM; JEOL, JSM-6700F) with an accelerating voltage of 5 kV. X-ray photoelectron spectroscopy (XPS) measurements were recorded on a Thermo Scientific K-Alpha spectrometer operating with an unmonochromatized Al Kα X-ray source. The data were calibrated by the binding energy of C1s (284.6 eV). The ions dissolved in the electrolyte after the stability testing were measured by inductively coupled plasma atomic emission spectroscopy (ICP-AES; Option-5300DV, PerkinElmer, USA).

2.4 PEC characterization

PEC characterization was carried out in 0.1 M potassium phosphate aqueous solution buffered to pH 5.5. The electrolyte was purged with Ar for 30 min before PEC measurements. The properties of the separate electrodes were tested in a three-electrode cell using an electrochemical analyzer (CHI-630D, Chenhua Co., China). Pt foil and a saturated calomel electrode (SCE) were used as the counter and reference electrodes, respectively. The potentials of the working electrode (V_{RHE}, reversible hydrogen electrode) were calculated by the formula:

$$V_{RHE}=V_{SCE}+0.059pH+E_{SCE}=V_{SCE}+0.5657 \quad (1)$$

Two-electrode measurements were conducted by connecting the working electrode lead of the potentiostat to the $BiVO_4$ photoanode and the reference and counter electrode leads to the Si nanoarray photocathode. An AM 1.5G sunlight (100 mW cm^{-2}) simulator (Oriel 92251A-1000) was used as the light source. The irradiated area was 0.28 cm^2 and photocurrent densities were normalized to 1 cm^2. Cyclic voltammetry was performed with a scan rate of 30 mV s^{-1}. Supposing that the Faradic efficiency is 100%, the STH conversion efficiency (η) may be calculated using the formula:

$$\eta=J_{SC}\ (\text{mA cm}^{-2}) \times 1.23\ (\text{V})/100\ (\text{mW cm}^{-2}) \quad (2)$$

Where J_{SC} is the photocurrent density of the two-electrode system (at 0 V_{RHE}) under AM 1.5G illumination (100 mW cm^{-2}).

3. Results and discussion

In a p/n PEC tandem cell, the $BiVO_4$ photoanode and Si nanoarray photocathode should be energetically matched to allow Z-scheme water splitting. [1] Fig. 1 shows the expected electron energetics of a $BiVO_4$/Si nanoarray-based tandem cell device without external bias. The conduction band of the photocathode and the valence band of the photoanode must lie across the water reduction and oxidation potentials to overcome the required 1.23 eV.[24] In addition, the tandem cell is theoretically possible only if the conduction band of the photoanode lies at lower electrochemical potential than the valence band of the photocathode. Next, the absorption

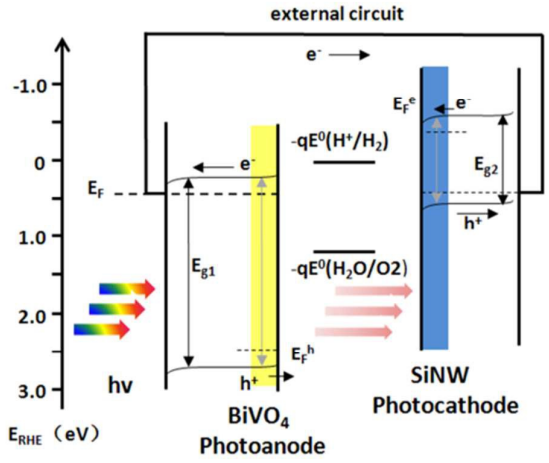

Fig. 1 Simplified electron energy diagram of a $BiVO_4$/Si nanoarray tandem cell for overall water splitting. The cell is shown in the wired configuration under illumination with approximated positions of the Fermi energy, E_F, and the minority carrier quasi Fermi energies at the semiconductor–electrolyte interface.

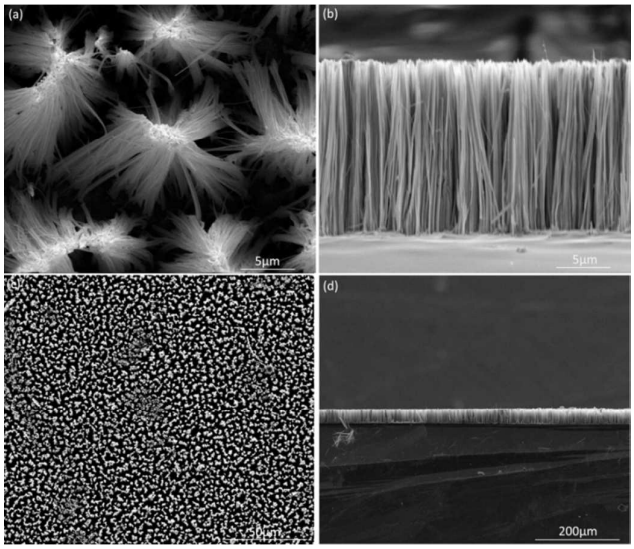

Fig. 2 Surface (a,c) and cross-sectional (b,d) SEM images of an as-prepared Si nanoarray. Scale bars: 5 μm for (a) and (b); 50 μm for (c); 200 μm for (d).

spectra of the two photoelectrodes should be suitably matched with solar photocurrent density. [24] When two photoelectrodes are wired together, the operating current density is decided by the photoelectrode that produces the smaller photocurrent. $BiVO_4$ has a band gap of ~2.4 eV, which is larger than that of the Si nanoarray (~1.12 eV). Therefore, when $BiVO_4$ is directly exposed to AM 1.5G illumination, it can potentially absorb all solar photons with wavelength λ up to ca. 510 nm, which corresponds to a maximum possible solar photocurrent density of 7.08 mA cm^{-2} (supposing that the incident photon-to-current efficiency (IPCE) is unity). If each of the photons not absorbed by $BiVO_4$ is incident on the photocathode surface, the p-Si nanoarray would absorb every photon with λ between 510 and 1107 nm. This corresponds to a maximum solar photocurrent density of 28.65 mA cm^{-2} assuming that the IPCE is unity. Thus, when the two electrodes with the same active areas are wired together, the water splitting photocurrent of the system should correspond to the ideal case of the $BiVO_4$ photoanode, with a maximum value of 7.08 mA cm^{-2} (STH conversion efficiency of ca. 8.7%). Although this is only an analysis of the ideal situation, the combination of $BiVO_4$ with Si nanoarrays is a reasonable possibility for an effective p-n tandem cell.

SEM images of a highly oriented p-Si nanoarray fabricated directly on a Si wafer by metal-catalyzed electroless etching are depicted in Fig. 2. The Si nanoarray contains congregated bundles of Si nanowires (SiNWs). The diameter of the SiNWs is in the range of 100–250 nm, and their length is about 15–20 μm. Fig. 2b shows the cross-section of a Si nanoarray in which all SiNWs are distinguishable, and most are oriented vertical to the wafer surface. The large-scale cross-section image in Fig. 2d confirms that the SiNWs are uniform over the entire wafer surface. The reason for the congregated bundles of SiNWs is that forces such as electrostatic charge and dangling bonds on the freshly formed surfaces induce mutual attraction of the SiNWs. Some scattered SiNWs are also present from cutting and loading the sample. The vertical orientation of the SiNWs is an advantage because the orthogonal directions of light absorption and minority-carrier collection mean that minority carriers only need to travel a short distance across the diameter of the SiNW before being collected at the electrode/electrolyte junction, compared with in a planar structure. This preferred geometry decreases reflection and scattering losses and allows the electrolyte to easily diffuse within the Si nanoarray, which increases the contact area between electrolyte and electrode, as well as the catalyst loading per unit area. [47, 48] An Mo-doped $BiVO_4$ photoanode was synthesized by a modified metal–organic decomposition method based on our previous work. [37] The X-ray diffraction pattern of this $BiVO_4$ photoanode is presented in Fig. S1, ESI†.

Next we examine the individual (three-electrode) current density–voltage (*J*–V) curves of the respective photoelectrodes in the tandem cell to better estimate the expected tandem cell operating point. Cobalt-based catalyst Co-Pi was deposited on the photoanode surface to minimize the overpotential using photoassisted galvanostatic electrodeposition with a fixed current of 10 μA. [46] The *J*–V curves of the $BiVO_4$ photoanode under simulated AM 1.5G irradiation in pH 5.5 potassium phosphate-buffered electrolyte are depicted in Fig. 3a. The Co-Pi/$BiVO_4$ photoanode showed a photocurrent onset at +0.3 V_{RHE}, and the photocurrent density was about 1.5 mA cm^{-2} at +0.5 V_{RHE}, which is about the position of the conduction band of Si (~0.5 V_{RHE}). Fig. 3b shows the *J*–V curves of a Pt-decorated Si nanoarray photocathode exposed to light filtered through the $BiVO_4$ photoanode in the same electrolyte. The presence of Pt electrocatalyst in the Pt/Si nanoarray electrode shifted

the onset potential for H_2 evolution by approximately 400 mV to ca. 0.35 V_{RHE}.

Comparing the *J*–V curves of the photoanode and photocathode provides further insight into the operation of the tandem cell. When the photoelectric properties of each electrode were measured under the same conditions (e.g., illumination, electrolyte), the operating point is where the absolute values of the (three-electrode) *J*–V curves for the photoanode and photocathode intersect. [17, 24] To find this point, we overlaid the absolute values of the *J*–V curve for the Si nanoarray photocathode exposed to light filtered through the $BiVO_4$ photoanode, as shown in Fig. 3c. The intersection point gave an operating point with a photocurrent density of 0.6 mA cm^{-2} (representing an STH conversion efficiency of 0.74%) and operating voltage of +0.38 V_{RHE}, which is close to the equilibrium Fermi energy of +0.4 V_{RHE} predicted from the flat-band potentials and band-edge energies shown in Fig. 1. The similar operating voltage and onset potential of the Si nanoarray reflect the fact that the predicted tandem cell current density is determined more strongly by the photocurrent density of the $BiVO_4$ photoanode close to its onset potential than by that of the Si nanoarray.

This nonzero operating point indicates the possibility of unassisted solar water splitting in a two-electrode tandem cell, despite the transmission loss of photons and unfavourable onset of both photoelectrodes. And then, we assembled the photoanode and photocathode in the two-electrode system without a reference electrode (Fig. S2, ESI†). Fig. 4a reveals that the short-circuit current density J_{sc} is 0.46 mA cm^{-2} (STH conversion efficiency of 0.57%), which is a little bit lower than the intersection point photocurrent and may originate from

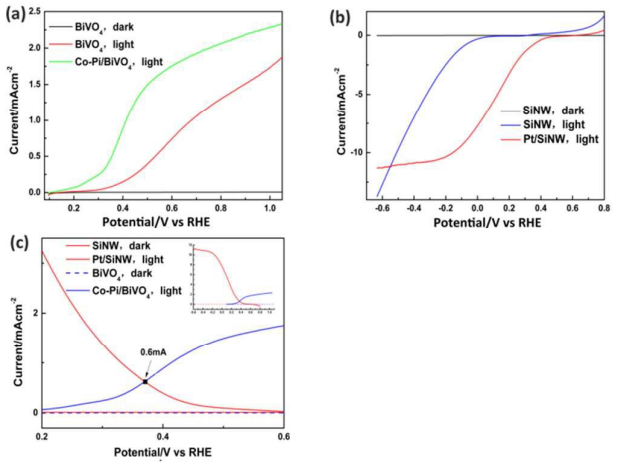

Fig. 3 *J*-V curves of (a) bare and Co-Pi-decorated $BiVO_4$ photoanodes, (b) bare and Pt-decorated Si nanoarray photocathodes exposed to light filtered through a $BiVO_4$ photoanode in aqueous 0.1 M potassium phosphate solution buffered to pH 5.5 under AM 1.5G sunlight illumination (100 mW cm^{-2}), and (c) intersection point of the *J*-V curves of the two types of electrodes.

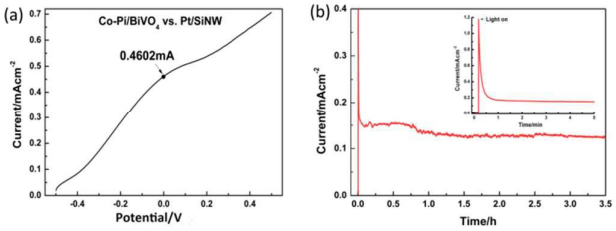

Fig. 4 (a) *J*–V curve of the two-electrode system Co-Pi/Mo:$BiVO_4$ against the Pt/p-Si nanoarray photocathode, (b) Photocurrent of the two-electrode $BiVO_4$/Si nanoarray tandem cell with no applied bias under AM 1.5G sunlight illumination (100 mW cm^{-2}).

series resistance. The stability of the tandem cell was tested without external bias for 3.5 h, as shown in Fig. 4b. The tandem cell exhibited a transient current spike upon turning on the simulated illumination because of capacitive charging effects. [49] After 100 s of operation, a photocurrent density of ca. 0.16 mA cm^{-2} (STH conversion efficiency of 0.2%) was observed for the $BiVO_4$/Si nanoarray tandem cell. The cell reached a stable photocurrent density of ca. 0.12 mA cm^{-2} (STH conversion efficiency of 0.15%) after 3.5 h, which was lower than the value predicted by the operating point. This suggests that a considerable loss occurs or instability exists in the tandem cell.

One of the potential losses of the cell arose from the pH gradient that developed near the electrodes, which was not considered by the intersecting point analysis. [50] Even though the bulk electrolyte was buffered at near-neutral pH (5.5), the consumption of protons at the cathode and liberation of protons at the anode during operation of the system would drive the local pH near the electrodes to more alkaline or acidic values, which caused an additional voltage loss, E_{pH}. [51] Upon rerunning the *J*–V analysis of the $BiVO_4$ photoanode and Si nanoarray photocathode after use in the tandem cell, the two electrodes showed opposite *J*–V behaviours (Fig. S3, ESI†). In contrast to performance degradation originating from oxidation of Si, which is often taken for granted, the photocurrent density of Si nanoarray photocathode was enhanced after the stability testing. In addition, the onset potential, which is crucial to the performance of the tandem cell, was identical to that of the electrode before the stability testing (Fig. S3b, ESI†).

To eliminate the influences of electrocatalyst and surface morphology on the PEC performance, we measured the stability and *J*-V properties of a bare planar p-Si electrode and bare p-Si nanoarray electrode in a three-electrode cell (Fig. S4 and S5, ESI†). After 1 h of stability testing, both of the electrodes showed improvements in the photocurrent density and the onset potential. XPS was then used to study the chemical nature of Si on the surface of electrodes (Figs. S6 and S7, ESI†). The binding energy of Si $2p_{3/2}$ on the surface of the electrodes before and after the stability testing showed a slight shift caused by a change of chemical environment. Group states of Si and H will shift binding energies to higher energy. Generally, each additional H atom shifts the energy of

Si 2p by ΔEn=(0.34±0.1) eV. [52] Therefore, the observed shift may indicate the presence of groups like SiH and SiH_2 on the surface of the Si photocathode. Surface states often act as recombination centers for photogenerated electron–hole pairs. After the stability testing, most of the surface recombination centers are eliminated. This may explain why the photocurrent of the Si electrode increases following stability testing. Additionally, in the reducing environment near the photocathode, the SiO_2 oxide layer might gradually corrode, which would improve the conductivity of the electrode. Regardless of the mechanism, the stability of the p-Si nanoarray does not limit the performance of the tandem cell.

In contrast, both the photocurrent and onset potential of the $BiVO_4$ electrode decreased after the stability testing. Considering the buildup of local pH gradients discussed above, we speculate that some corrosion and dissolution may occur on the electrode surface. ICP-AES was used to measure the possible dissolution of metal ions after the stability testing; the results are summarized in Tab. S1, ESI†. The amount of Bi^{3+} and V^{5+} in the electrolyte before and after the stability testing barely changed, but the amount of Co^{2+} increased from 0.009 mg/L to 0.27 mg/L, which indicates that the catalyst corroded during the stability testing. It is well known that at low operating voltages on dark electrodes, the catalyst "repair" mechanism of Co^{2+} does not occur at a sufficient rate (in our case, the operating voltage of the tandem cell was less than 0.4 V_{RHE}), which leads to poor stability of the Co-Pi layer. [53,54] The low current density and pH gradient could also accelerate catalyst dissolution. Increasing the pH of the electrolyte could somewhat ameliorate the dissolution of the Co-Pi catalyst. However, the Si nanoarray photocathode gives a better onset potential under lower pH (Fig. S8, ESI†). The trade-off between high pH to improve Co-Pi catalyst stability and low pH to minimize the photocathode onset potential presents a major challenge to realize a stable Co-Pi-catalyzed $BiVO_4$/Si nanoarray tandem cell.

4. Conclusions

In this study, we designed and fabricated a $BiVO_4$/Si nanoarray photoanode/photocathode tandem device for unassisted overall solar water splitting. Theoretically, a maximum STH conversion efficiency of 8.7% may be obtained with this promising combination in ideal case. Although the catalysts for water oxidation and reduction have been used, the low fill factor and nonideal onset-potentials of both photoelectrodes decreased the actual conversion efficiency of the device. Despite these losses, the two-electrode p-n tandem cell reached a solar photocurrent density of 0.46 mA cm^{-2} with no applied bias, representing an STH conversion efficiency of 0.57%. The decay of transient photocurrents in minutes is caused by the dissolution of Co-Pi electrocatalyst as the pH of the electrolyte must give consideration to both electrodes. To increase the STH conversion efficiency, further optimization should focus on appropriate material selection to make sure that the conduction band of that photoanode lies at sufficiently lower electrochemical potential than the valence band of the photocathode to accommodate the onset-potentials of both photoelectrodes.

Acknowledgements

This work was supported by the National Basic Research Program of China (2013CB632404), a Project Funded by the Priority Academic Program Development of Jiangsu Higher Education Institutions, New Century Excellent Talents in University (NCET-12-0268), and the National Natural Science Foundation of China (Nos. 21473090 and 51272102).

References

1 M. Grätzel, *Nature*, 2001, **414**, 338.
2 Z. S. Li, J. Y. Feng, S. C. Yan and Z. G. Zou, *Nano Today*, 2015, **10**, 468.
3 M. Zhou, X. W. Lou and Y. Xie, *Nano Today*, 2013, **8**, 598.
4 J. Y. Feng, W. J. Luo, T. Fang, H. Lv, Z. Q. Wang, J. Gao, W. M. Liu, T. Yu, Z. S. Li and Z. G. Zou, *Adv. Funct. Mater.*, 2014, **24**, 3535.
5 S. J. A. Moniz, S. A. Shevlin, D. J. Martin, Z. –X. Guo and J. W. Tang, *Energy Environ. Sci.*, 2015, **8**, 731.
6 M. J. Liao, J. Y. Feng, W. J. Luo, Z. Q. Wang, J. Y. Zhang, Z. S. Li, T. Yu and Z. G. Zou, *Adv. Funct. Mater.*, 2012, **22**, 3066.
7 J. Y. Feng, D. P. Cao, Z. Q. Wang, W. J. Luo, J. J. Wang, Z. S. Li and Z. G. Zou, *Chem. Eur. J.*, 2014, **20**, 16384.
8 K. Sun, S. H. Shen, Y. Q. Liang, P. E. Burrows, S. S. Mao and D. L. Wang, *Chem. Rev.*, 2014, **114**, 8662.
9 M. G. Walter, E. L. Warren, J. R. McKone, S. W. Boettcher, Q. Mi, E. A. Santori and N. S. Lewis, *Chem. Rev.*, 2010, **110**, 6446.
10 T. Hisatomi, J. Kubota and K. Domen, *Chem. Soc. Rev.*, 2014, **43**, 7520.
11 M. L. Zhang, W. J. Luo, Z. S. Li, T. Yu and Z. G. Zou, *Appl. Phys. Lett.*, 2010, **97**, 042105.
12 J. R. Bolton, S. J. Strickler and J. S. Connolly, *Nature*, 1985, **316**, 495.
13 Z. S. Li, W. J. Luo, M. L. Zhang, J. Y. Feng and Z. G. Zou, *Energy Environ. Sci.*, 2013, **6**, 347.
14 Y. Pihosh, I. Turkevych, K. Mawatari, J. Uemura, Y. Kazoe, S. Kosar, K. Makita, T. Sugaya, T. Matsui, D. Fujita, M. Tosa, M. Kondo and T. Kitamori, *Sci. Rep.* 2015, **5**, 11141.
15 Y. -S. Chen, J. S. Manser and P. V. Kamat, *J. Am. Chem. Soc.*, 2015, **137**, 974.
16 L. Han, F. F. Abdi, R. van de Krol, R. Liu, Z. Huang, H. –J. Lewerenz, B. Dam, M. Zeman and A. H. M. Smets, *ChemSusChem*, 2014, **7**, 2832.
17 J. Brillet, M. Cornuz, M. Grätzel and K. Sivula, *J. Mater. Res.* 2010, **25**, 17.
18 J. H. Kim, Y. Jo, J. H. Kim, J. W. Jang, H. J. Kang, Y. H. Lee, D. S. Kim, Y. Jun and J. S. Lee, *ACS Nano*, 2015, DOI: 10.1021/acsnano.5b03859
19 L. Andrade, R. Cruz, H. A. Ribeiro and A. Mendes, *Int. J. Hydrogen Energy*, 2010, **35**, 8876
20 X. Shi, K. Zhang, K. Shi, M. Ma, J. Kwon, I. T. Choi, J. K. Kim, H. K. Kim, D. H. Wang and J. H. Park, *Nano Energy*, 2015, **13**, 182.
21 C. M. Ding and C. Li, *Phys. Chem. Chem. Phys.*, 2014, **16**, 15608.
22 O. Khaselev and J. A. Turner, *Science*, 1998, **280**, 425.

23 F. F. Abdi, L. Han, A. H. Smets, M. Zeman, B. Dam and R. van de Krol, *Nat. Commun.*, 2013, **4**, 2195.
24 P. Bornoz, F. F. Abdi, S. D. Tilley, B. Dam, R. van de Krol, M. Graetzel and K. Sivula, *J. Phys. Chem. C*, 2014, **118**, 16959.
25 L. Tong and A. J. Mozer, *Energy Environ. Sci.*, 2012, **5**, 9472.
26 A. J. Nozik, *Appl. Phys. Lett.*, 1976, **29**, 150.
27 H. B. Yang, J. W. Miao, S. –F. Hung, F. W. Huo, H. M. Chen, B. Liu, *ACS Nano*, 2014, **8**, 10403.
28 M. J. Kenney, M. Gong, Y. Li, J. Z. Wu, J. Feng, M. Lanza and H. Dai, *Science*, 2013, **342**, 836.
29 J. Yang, K. Walczak, E. Anzenberg, F. M. Toma, G. Yuan, J. Beeman, H. Frei and I. D. Sharp, *J. Am. Chem. Soc.*, 2014, **136**, 6191.
30 E. L. Miller, D. Paluselli, B. Marsen and R. E. Rocheleau, *Sol. Energy Mater. Sol. Cells.*, 2005, **88**, 131.
31 S. W. Boettcher, E. L. Warren, M. C. Putnam, E. A. Santori, D. Turner-Evans, M. D. Kelzenberg, M. G. Walter, J. R. McKone, B. S. Brunschwig, H. A. Atwater and N. S. Lewis N S, *J. Am. Chem. Soc.*, 2011, **133**, 1216.
32 S. W. Boettcher, J. M. Spurgeon, M. C. Putnam, E. L. Warren, D. B. Turner-Evans, M. D. Kelzenberg, J. R. Maiolo, H. A. Atwater and N. S. Lewis, *Science*, 2010, **327**, 185.
33 S. Haussener, C. Xiang, J. M. Spurgeon, S. Ardo, N. S. Lewis and A. Z. Weber, *Energy Environ. Sci.*, 2012, **5**, 9922.
34 B. M. Kayes, H. A. Atwater and N. S. Lewis, *J. Appl. Phys.*, 2005, **97**, 114302.
35 M. H. Lee, J. W. Ager and A. Javey, *Angew. Chem. Int. Ed.*, 2012, **51**, 10760.
36 J. R. Maiolo, B. M. Kayes, M. A. Filler, H. A. Atwater and N. S. Lewis, *J. Am. Chem. Soc.*, 2007, **129**, 12346.
37 W. J. Luo, Z. S. Yang, Z. S. Li, J. Y. Zhang, J. G. Liu, Z. Y. Zhao, Z. Q. Wang, S. C. Yan, T. Yu and Z. G. Zou, *Energy Environ. Sci.*, 2011, **4**, 4046.
38 M. Zhou, H. B. Wu, J. Bao, L. Liang, X. W. Lou and Y. Xie, *Angew. Chem. Int. Ed.*, 2013, **52**, 8679.
39 W. J. Luo, Z. S. Li, T. Yu and Z. G. Zou, *J. Phys. Chem. C.*, 2012, **116**, 5076.
40 A. Fujishima and K. Honda, *Nature*, 1972, **238**, 37.
41 D. P. Cao, W. J. Luo, J. Y. Feng, X. Zhao, Z. S. Li and Z. G. Zou Z G, *Energy Environ. Sci.*, 2014, **7**, 752.
42 C. Santato, M. Ulmann and J. Augustynski, *J. Phys. Chem. B*, 2011, **105**, 936.
43 K. Q. Peng and S. T. Lee, *Adv. Mater.*, 2011, **23**, 198.
44 H. Fang, Y. Wu, J. H. Zhao and J. Zhu, *Nanotechnology*, 2006, **17**, 3768.
45 J. R. McKone, E. L. Warren, M. J. Bierman, S. W. Boettcher, B. S. Brunschwig, N. S. Lewis N S and H. B. Gray, *Energy Environ. Sci.*, 2011, **4**, 3573.
46 K. P. Satyananda, E. F. Thomas, D. B. Logan, G. D. Todd, A. T. John and M. H. Andrew, *Energy Environ. Sci.*, 2011, **4**, 5028.
47 E. L. Warren, J. R. McKone, H. A. Atwater, H. B. Gray and N. S. Lewis, *Energy Environ. Sci.*, 2012, **5**, 9653.
48 J. M. Rubi and S. Kjelstrup, *J. Phys. Chem. B*, 2003, **107**, 13471.
49 F. Le Formal F, K. Sivula and M. Grätzel, *J. Phys. Chem. C*, 2012, **116**, 26707.
50 E. A. Hernandez-Pagan, N. M. Vargas-Barbosa, T. Wang, Y. Zhao, E. S. Smotkin and T. E. Mallouk, *Energy Environ. Sci.*, 2012, **5**, 7582.
51 J. Jin, J. Walczak, N. S. Lewis and C. X. Xiang, *Energy Environ. Sci.*, 2014, **7**, 3371.
52 L. LEY, *The Physics of Hydrogenated Amorphous Silicon II Applied Physics*, 1984, **56**, 61.
53 Y. Surendranath, D. A. Lutterman, Y. Liu and D. G. Nocera, *J. Am. Chem. Soc.*,2012, **134**, 6326.
54 D. A. Lutterman, Y. Surendranath and D. G. Nocera, *J. Am. Chem. Soc.*, 2009, **131**, 3838.